Integrated Randomized and Cell Surface-Informed Peptide Libraries Enable Tissue-Tropic AAV Capsid Evolution

Qingyu Deng, Yangyang Zhong, Ruixue Chen, Yan Jiao, Ying Bai, Gang Wang

Byongen Therapeutics, Beijing, China Correspondence: gang.wang@byongen.com

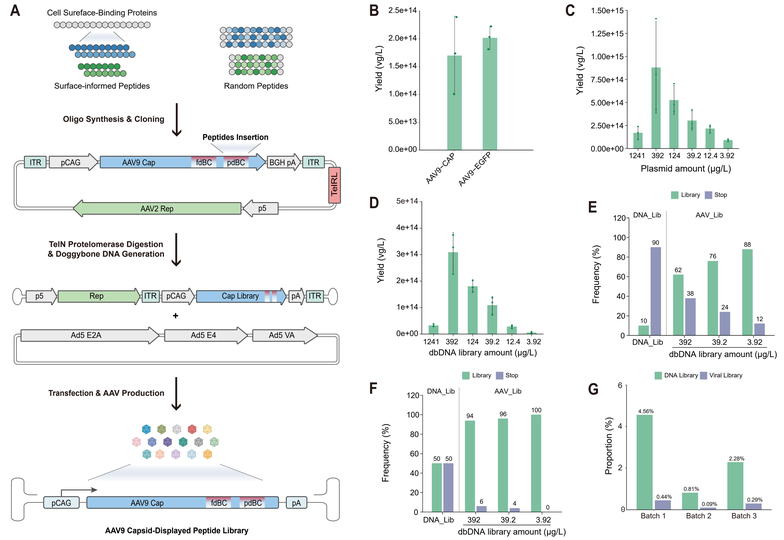
ASGCT 29th Annual Meeting
Poster Number, 2029

INTRODUCTION

Directed evolution of AAV capsids is critical for optimizing adeno-associated virus (AAV) vectors for gene therapy. A common strategy involves inserting randomized peptides into specific capsid variable regions (VRs) to evolve variants with enhanced tissue tropism. More recently, libraries derived from proteins known to interact with cell surface receptors have emerged as a complementary approach. We developed PEARS (Peptide-driven Evolution of AAV via Randomized and Surface-informed libraries) to combine the advantages of both strategies. PEARS integrates a fully randomized peptide library with a surface-informed library derived from diverse cell surface-interacting proteins. By combining optimized capsid library production with RNA-Seq-based in vivo screening, PEARS enables rapid, high-throughput directed evolution of AAV variants across multiple organs.

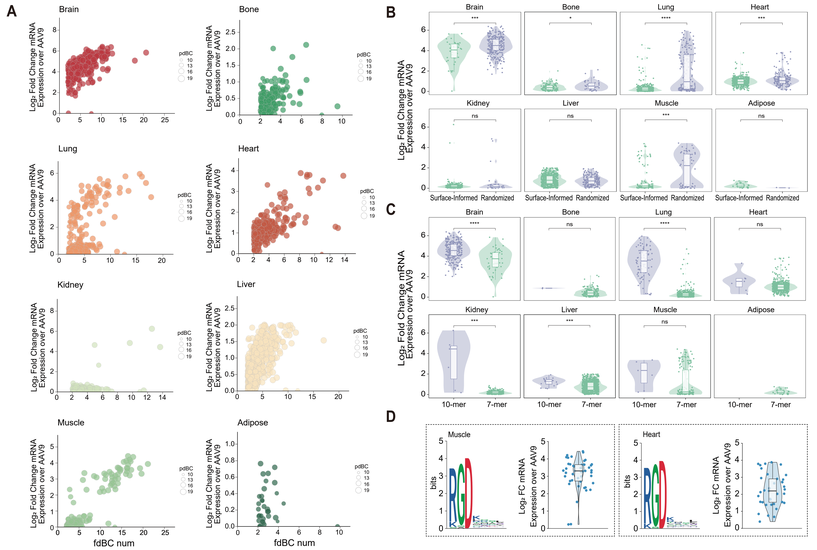
RESULTS

Figure 1. PEARS Platform Design and Optimization



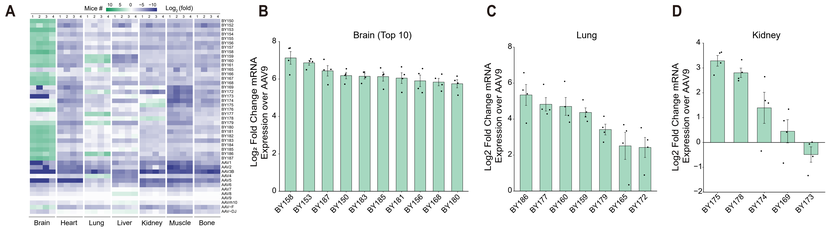
(A) The PEARS platform employs a dual-library design of randomized and surface-informed 7/10-mer peptides, the latter featuring ~4 million unique sequences from 15,000 surface proteins. Peptides were inserted into the VR-VIII region of the capsid backbone. A synergistic tracking system, integrating upstream fdBC (flanking degenerate barcode) and internal pdBC (peptide degenerate barcode) via synonymous codon degeneracy, assigns a unique DNA identifier to each variant for precise quantification and tracing. The TelN/TelRL system converted circular plasmids into linear dbDNA, which was co-transfected with a helper plasmid (dual-DNA packaging) for AAV production. (B) Yield comparison between dual-DNA and triple-plasmid systems under standard conditions (1,241 μg/L Rep/Cap). (C–D) Dosage optimization for (C) CAP-plasmid and (D) dbDNA library. Both achieved peak titers at 392 μg/L, outperforming standard dosages. (E–F) Packaging fidelity and cross-packaging analysis. Frequency of functional library sequences versus defective variants (indicated as “Stop”, representing sequences with premature stop codons) across various dbDNA concentrations. A dosage of 39.2 μg/L was selected as the optimal threshold to effectively balance viral yield and packaging fidelity. (G) Quality control analysis. A 7.9–10.4-fold reduction in defective sequences was observed in the viral library relative to the initial DNA library across three independent 1 L production batches, demonstrating the high purity and consistency of the optimized production platform.

Figure 2. In Vivo Screening Landscape and Structural Determinants of AAV Tropism Across Tissues



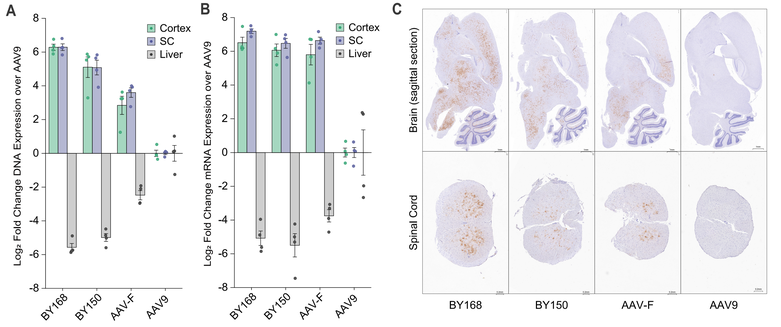
(A) Tissue-specific profile. Log2 fold change of ~1,000 variants relative to AAV9 demonstrated superior transduction performance in the brain and lung, followed by the kidney. Moderate increases occurred in heart and muscle, while the lowest levels were observed in liver, bone, and adipose tissue. (B) Design strategy. Randomized variants outperformed in the brain and lung, whereas surface-informed variants exhibited preferential gains in the liver, kidney, and adipose tissue. This divergence underscores the necessity of a dual-library approach, as each strategy offers complementary advantages for targeting distinct organ systems. (C) Peptide length. Evaluation revealed a length-dependent tropism: 10-mers favored the brain, lung, and kidney, while 7-mers were more effective in targeting the heart, muscle, and bone. (D) Motif-level determinants. The RGD motif was identified as a key driver for cardiac and skeletal muscle targeting.

Figure 3. Barcode-Based In Vivo Validation of Tissue-Tropic AAV Variants



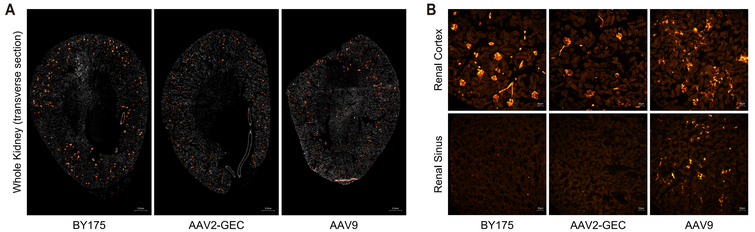
(A) In vivo validation. Heatmap showing log2 fold changes in mRNA expression for 32 candidates (20 brain, 7 lung, 5 kidney-derived) and controls relative to AAV9. (B–D) Comparative performance. Ranked bar plots of lead AAV candidates in (B) brain (top 10), (C) lung, and (D) kidney relative to AAV9. Most variants showed significantly enhanced efficiency, consistent with organ-specific tropism profiles from initial screening.

Figure 4. Randomized Screening Identifies Superior CNS-Tropic Variants BY168 and BY150



(A, B) Relative viral genome copies (A) and mRNA expression (B) of variants in the cortex, spinal cord (SC), and liver of BALB/c mice (n = 4), 3 weeks after intravenous injection (1.5×10^{13} vg/kg). Data are presented as log2 fold change normalized to AAV9. The results showed that BY168, identified from the random library, significantly outperformed AAV-F, exhibiting up to 146-fold increase in spinal cord mRNA and up to 78-fold increase in cortex/spinal cord DNA compared to AAV9, coupled with >97% liver de-targeting. (C) Representative GFP immunohistochemistry staining of sagittal brain sections (scale bar, 1 mm) and spinal cord cross-sections (scale bar, 0.2 mm) from mice treated with BY168, BY150, AAV-F, and AAV9. Immunohistochemistry further confirmed BY168 as the most potent variant, demonstrating robust and widespread GFP expression throughout the brain and spinal cord.

Figure 5. Surface-Informed Screening Identifies BY175 with Potent Renal Vascular Tropism



(A) Whole-kidney biodistribution. Representative immunofluorescence scans of GFP expression in BALB/c mice (n=4) three weeks post-intravenous injection (1.5×10^{13} vg/kg) of BY175, AAV2-GEC, and AAV9. Scale bar, 0.5 mm. (B) High-magnification cortex and sinus imaging. BY175 and AAV2-GEC predominantly transduced the cortical vascular endothelium (including glomeruli and cortical vessels). In contrast, AAV9 exhibited an interstitial pattern, characteristic of mesangial or fibroblast targeting. Scale bar, 50 μm. Together, these results showed that surface-informed BY175 had superior vascular endothelial tropism over AAV2-GEC, yet a distinct profile from AAV9.

CONCLUSION

>> PEARS demonstrated that AAV performance is driven by the interplay of design strategy, peptide length, and tissue type. Combining randomized and surface-informed libraries maximizes the discovery of diverse, high-performance variants.

>> In vivo validation confirmed PEARS’ ability to isolate high-performance variants. BY168 achieves robust CNS transduction with minimal liver sequestration, while BY175 exhibits potent, specific targeting of the renal cortical vascular endothelium.